Acta Mech Sin (2008) 24:161–169
DOI 10.1007/s10409-007-0131-0

RESEARCH PAPER

Coarse grained molecular dynamics and theoretical studies of carbon nanotubes entering cell membrane

Xinghua Shi · Yong Kong · Huajian Gao

Received: 24 October 2007 / Revised: 16 November 2007 / Accepted: 16 November 2007 / Published online: 6 March 2008

Abstract Motivated by recent experimental observations that carbon nanotubes (CNT) can enter animal cells, here we conduct coarse grained molecular dynamics and theoretical studies of the intrinsic interaction mechanisms between CNT's and lipid bilayer. The results indicate that CNT-cell interaction is dominated by van der Waals and hydrophobic forces, and that CNT's with sufficiently small radii can directly pierce through cell membrane while larger tubes tend to enter cell via a wrapping mechanism. Theoretical models are proposed to explain the observed size effect in transition of entry mechanisms.

Keywords Molecular dynamics · Carbon nanotube · Cell membrane · Interaction mechanism

1 Introduction

The question of whether and how nanomaterials enter human and animal cells is a significant issue for the development of efficient gene and drug delivery systems as well as for assessing the potential hazards of nanotechnology on ecology and human health. Due to their unique physical, chemical, electrical and optical properties, carbon nanotubes (CNT) and other nanomaterials have shown enormous potential and promise to be adapted and integrated into biomedical devices, such as site-specific drug delivery systems [1–3], non-viral gene carriers [4] as well as biosensor and screening systems [5–7]. Along with these promising applications, there is also increasing concern about the effects of nanomaterials on human health. For example, in assessing responses of animal/human cells to CNT's, it was found that some cells tend to wrap CNT's into nodular structures and isolate CNT-attached parts from the main cell population [8]. It has also been convincingly shown that CNT's can cross the cell membrane into cytoplasm, even entering cell nucleus [9–16]. On the other hand, the mechanisms and pathways CNT's entering cells are not fully resolved. So far, two different uptake pathways have been suggested based on experimental observations: one is endocytosis [9–13] and the other is direct insertion and diffusion through the lipid bilayer of cell membrane [14–16]. Since the CNT's used in experiments are not pure and often functionalized in different ways, and cell membranes are chemically more complex than just lipids, relatively little is known about the intrinsic mechanism of interaction between CNT's and the lipid bilayer. Yet from a fundamental point of view, a first step to understand CNT-cell interaction mechanisms, and cellular responses to CNT's in general, should be to clarify how a CNT interacts with a pure lipid bilayer. For this problem, coarse grained molecular dynamics (CGMD) is a powerful tool of investigation.

In the present work, we conduct CGMD and theoretical studies to investigate how carbon nanotubes of different sizes interact and enter a patch of lipid bilayer. By reducing the number of degrees of freedom together with the use of short range potentials, CGMD models can gain four to five orders of magnitude in speed compared with full-atom models, achieving length scales on the order of micrometers and timescales on the order of milliseconds. Encouraged by such computational efficiency, a number of CGMD models have been developed and used to study lipids and surfactants systems, including micelles [17,18], bilayers [19,20],

X. Shi · H. Gao (✉)
Division of Engineering, Brown University, 182 Hope Street, Providence, RI 02912, USA
e-mail: Huajian_Gao@brown.edu

Y. Kong
ICx Radiation GmbH, Koelnerstrasse 99, 42651 Solingen, Germany

micelle aggregation [21] and vesicle formation [22]. However, it should be noted that the computational efficiency of CGMD models is usually gained at the cost of loss in accuracy. An optimal balance between efficiency and accuracy is a key aspect to the development and implementation of CGMD models. Recently, Marrink et al. [23] have developed a new CGMD model for lipid and surfactant systems, and it has been shown that this model gives quite accurate results for structural, elastic, dynamic as well as thermodynamic properties for a number of lipid systems. We will therefore adopt this model in our study.

2 Methods

2.1 Simulation model

In the CGMD model [23] adopted for the present study, nonbonded interactions between two particles are described by the Lennard-Jones (LJ) potential. The equilibrium distance between two particles is selected as 0.47 nm in all pair groups. The strength of the interaction, however, is set at five different levels, namely I ($\varepsilon = 5.0\,\mathrm{kJ\,mol^{-1}}$), II ($\varepsilon = 4.2\,\mathrm{kJ\,mol^{-1}}$), III ($\varepsilon = 3.4\,\mathrm{kJ\,mol^{-1}}$), IV ($\varepsilon = 2.6\,\mathrm{kJ\,mol^{-1}}$) and V ($\varepsilon = 1.8\,\mathrm{kJ\,mol^{-1}}$) [24]. A cutoff distance of 1.2 nm is selected for the LJ potential to smoothly shift to zero between the distance of 0.9 and 1.2 nm. Normal Coulombic potential is used for the electrostatic interaction. The bonded interaction is described by a harmonic potential with an equilibrium distance of 0.47 nm and a force constant of $1{,}250\,\mathrm{kJ\,mol^{-1}\,nm^{-2}}$. In our simulations, we select a bilayer of dipalmitoylphosphatidylcholine (DPPC) lipids, each lipid molecule consisting of 12 particles, two of which have attractive interaction (level I) with water molecules (hydrophilic head group), eight have repulsive interaction (level V) with water molecules (hydrophobic tail) and the other two have intermediate interaction (level III). Multi-walled nanotubes with radii from 1 to 5 nm and single-walled nanotubes with radii from 0.5 to 0.75 nm are constructed with the same length 6 nm. The multi-walled tubes are formed by assembling single-walled tubes with different radii with an inter-layer spacing of 0.68 nm (Fig. 1). The single-walled tube is constructed by folding a plane of rhombic cells, each cell consisting of four particles with the nearest neighbour distance 0.42 nm and internal angle 60°. In the multi-walled tubes, all the nearest and second nearest particles are connected through harmonic potential with a force constant equal to $300\,\mathrm{kJ\,mol^{-1}\,nm^{-2}}$, so that as a whole the tubes become almost rigid. Such multi-walled tubes can mimic hollow single wall tubes with closed ends and prevent unintended insertion of lipid molecules into the tubes. Since CNT's are commonly functionalized by binding with some proteins or other molecules on their surfaces to enhance their affinity with the cell, the interaction between

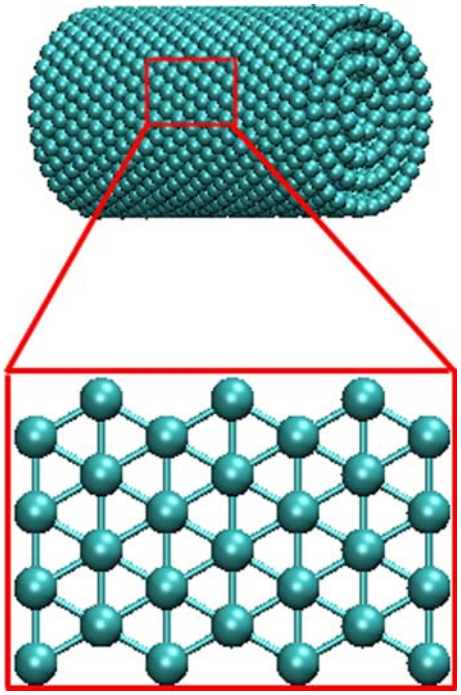

Fig. 1 Schematic illustration of a coarse grained model of multi-walled carbon nanotubes formed from several single-walled nanotubes with an inter-layer spacing of 0.68 nm. The single-walled nanotube is constructed by rolling up a plane composed of rhombic cells, each cell consisting of four particles with nearest neighbour distance 0.42 nm and internal angle 60°

tube particles and the head group of lipid molecules is set at level I. The interactions of tube particles with water and tails of lipid molecules are set at level III. All the parameters in the CGMD simulations are taken according to the above arrangement unless mentioned otherwise.

2.2 Simulation set-up

An equilibrated bilayer containing 128 DPPC lipids from Ref. [24] is copied seven times in two lateral directions to generate a patch of membrane consisting of 6,272 lipids with an in-plane lateral dimension of 42 nm × 42 nm. Initially, the nanotubes are arranged in close proximity above the center of the bilayer (at a distance of 1 nm to the bilayer surface) with tube axis perpendicular to the plane of the bilayer. Since living cells are usually covered with glycocalyx, a layer of polysaccharides on the outer membrane, we assume that, due to the lateral confinement of glycocalyx, the nanotubes would enter the lipid bilayer with their axis perpendicular to the layer. In the simulations, this lateral confinement is realized by constraining the lateral degrees of freedom. The bilayer and a selected nanotube are placed in a water box of volume 47 nm × 47 nm × 35 nm which contains 586,000 water particles (234,4000 water molecules). Periodic boundary condition is applied in three orthogonal directions. All

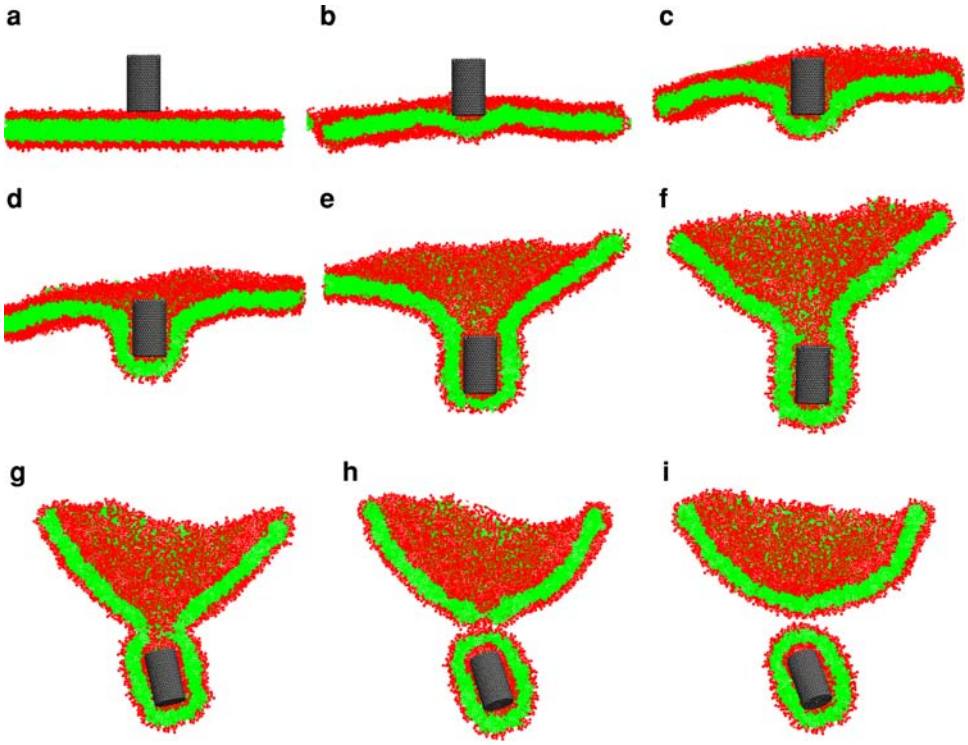

Fig. 2 **a–f** Time sequence of six snapshots of a multi-walled nanotube entering a membrane via a wrapping process driven by the van der Waals force. The *red particles* indicate the head group of lipid molecules. **g**, **h** Fusion of the membrane neck. **i** Separation of the lipid covered tube from the membrane

simulations reported in this paper are carried out in the NPT ensemble at temperature 323 K and pressure 1 atm. Through Berendsen's method [24], the temperature and pressure are scaled with time constants of 5 and 10 ps, respectively. In all systems, the time step is taken as 20 fs to keep the simulations stable. All simulations are performed with the molecular dynamics package GROMACS [25].

3 Results and discussion

3.1 Wrapping of nanotubes into membrane

To explore the interaction of multi-walled carbon nanotubes with membrane, we perform a series of CGMD simulations of nanotubes interacting with the lipid bilayer patch described above. Figure 2a–f show the time sequence of six snapshots of a selected nanotube with radius 2.3 nm being wrapped into the bilayer. For clarity, the water molecules are not shown here. The nanotube, initially arranged at a distance of 1 nm above the relaxed planar bilayer (Fig. 2a), is seen to approach and adhere to the bilayer, causing a small fluctuation as the lipid molecules spread onto the bottom surface of the nanotube (Fig. 2b). With more and more lipid molecules in the upper monolayer of the bilayer adhere to the tube, the bilayer changes its shape into an invagination to wrap around the tube (Fig. 2c–e). At the later stage of this wrapping process, the membrane near the top end of the tube forms a neck (Fig. 2f). To complete the wrapping process so that the tube can cross over to the other side of the membrane, the bilayer around the neck must fuse so that the lipid covered tube can detach from the membrane. This wrapping-fusion process is quite similar to budding/wrapping of viruses for which dynamics and other transmembrane proteins in the necked region are known to facilitate the detachment or fission process by reducing the binding affinity of membrane [26,27]. In the CGMD simulations, we mimic this process by reducing the interactions between lipid molecules at the neck region. Figure 2g, h show the fusion of bilayer and Fig. 2i shows the final state of the fission process, where the outer monolayer fuses and the lipid covered tube is completely separated from the membrane.

Figure 3 shows the variation of interaction energy between the tube and lipid molecules as a function of time. The steep slope of the energy profile in Fig. 3 indicates rapid wrapping at the initial stage. As the wrapping proceeds, the flattening of slope shows a gradual decrease of the wrapping speed. At the later stage, the increasing curvature deformation near the top end of the tube significantly slows down the wrapping process.

What is the driving force for wrapping the tube into the bilayer? As the particle forming the tube carries no electric charge, the tube interacts with lipid and water molecules primarily via van der Waals forces. To check the importance of van der Waals force in the wrapping process, we reduce the interaction strength between lipid and tube particles and repeat the simulation. The magenta line in Fig. 3 shows that, with 50% reduction in van der Waals interaction strength, the tube will adhere to the membrane but no wrapping occurs. Because the simulations are performed in a water box and

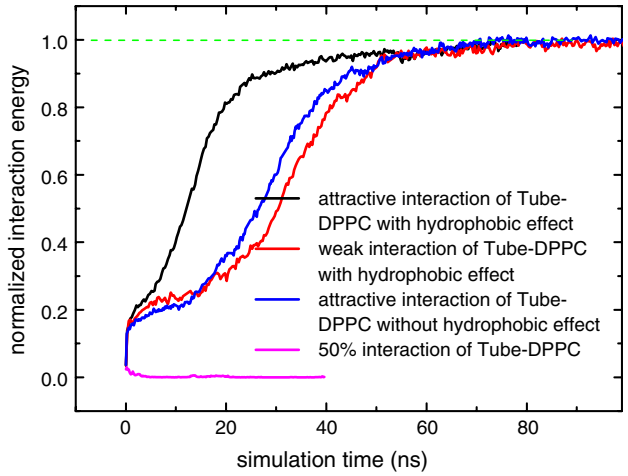

Fig. 3 Interaction energy (normalized by the maximum interaction energy with corresponding interaction parameters) between the nanotube and membrane as a function of simulation time. The *black line* shows the case of strong interaction between the nanotube and DPPC in the presence of hydrophobic effect. The *red line* shows the case of weak interaction between the nanotube and DPPC in the presence of hydrophobic effect on. The *blue line* shows the case of strong interaction between the nanotube and DPPC in the absence of hydrophobic effect. The *magenta line* corresponds to the case when the interaction between the nanotube and DPPC is reduced by 50%

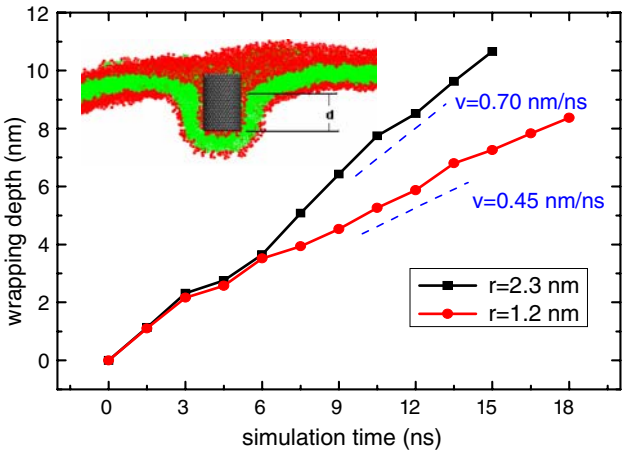

Fig. 4 The depth of wrapping as a function of simulation time. The wrapping velocity is about 0.7 nm/ns for a nanotube with radius 2.3 nm (*black line*) and about 0.45 nm/ns (*red line*) for a smaller tube with radius 1.2 nm

the carbon nanotubes are hydrophobic materials, how important is the hydrophobic effect in this process? To clarify this question, we change the interaction between water and tube molecules from level III to level IV and repeat the simulation. The blue line in Fig. 3 shows that the tube is rapidly wrapped into the membrane with significant reduction in wrapping time, indicating that the hydrophobic effect has a significant effect on the wrapping process. We have also considered the case when the interaction between lipid and tube molecules is changed to level II. The red line in Fig. 3 shows that the wrapping speed is initially slower but eventually catches up with the blue line. These studies indicate that both van der Waals attraction (between the tube and bilayer) and hydrophobic interaction (between the tube and water) play important roles in the wrapping process.

To investigate the effect of tube radius on the wrapping process, we consider a smaller nanotube with radius 1.2 nm and repeat the simulation. Figure 4 shows the wrapping depth as a function of simulation time. The wrapping rate is about 0.7 nm/ns for the 2.3 nm tube and about 0.45 nm/ns for the 1.2 nm tube. This size effect can be understood from the fact that the thinner tube causes larger curvature energy of the membrane which tends to resist the wrapping process.

3.2 Piercing of nanotube through membrane

As the radius of the nanotube is further decreased, we observe an interesting change of entry mechanism. For the wrapping process to be successful, the driving force due to van der Waals and hydrophobic interactions must exceed the resistance force due to the curvature energy of the membrane. For sufficiently small tubes, the driving force would become comparable to or smaller than the resistance force. To illustrate this, we repeat the simulation for a single-walled nanotube of 0.5 nm in radius while keeping all the other conditions identical to the previous simulations. Figure 5a–c show that, instead of crossing the membrane via wrapping, the tube simply pierces through the membrane. Our results also confirm the work by Lopez et al. [28] that a small radius tube (∼0.65 nm) with hydrophilic caps would insert into membrane and serve as a synthetic channel. Apparently, with decreasing radius, a nanotube would change its pathway of entry from wrapping to piercing.

When the tube becomes a transmembrane tube as shown in Fig. 5d, there is no more driving force for the tube to move further. On the other hand, living cells exist in a complicated chemical environment influenced greatly by the ion concentrations in solution. The osmotic gradients across the cell membrane are known to drive much of transmembrane transport. We modify the interaction between tube and water molecules on the lower side of the membrane to level II, thus artificially adding a potential gradient across the membrane. This potential is seen to drive the tube through the bilayer (Fig. 5e, f). Figure 6 shows the variation of the interaction energy between the tube and water molecules above and below the bilayer.

3.3 Theoretical models of wrapping and piercing mechanisms

To aid the understanding of the observed change in pathway of nanotubes entering cell, we propose two theoretical

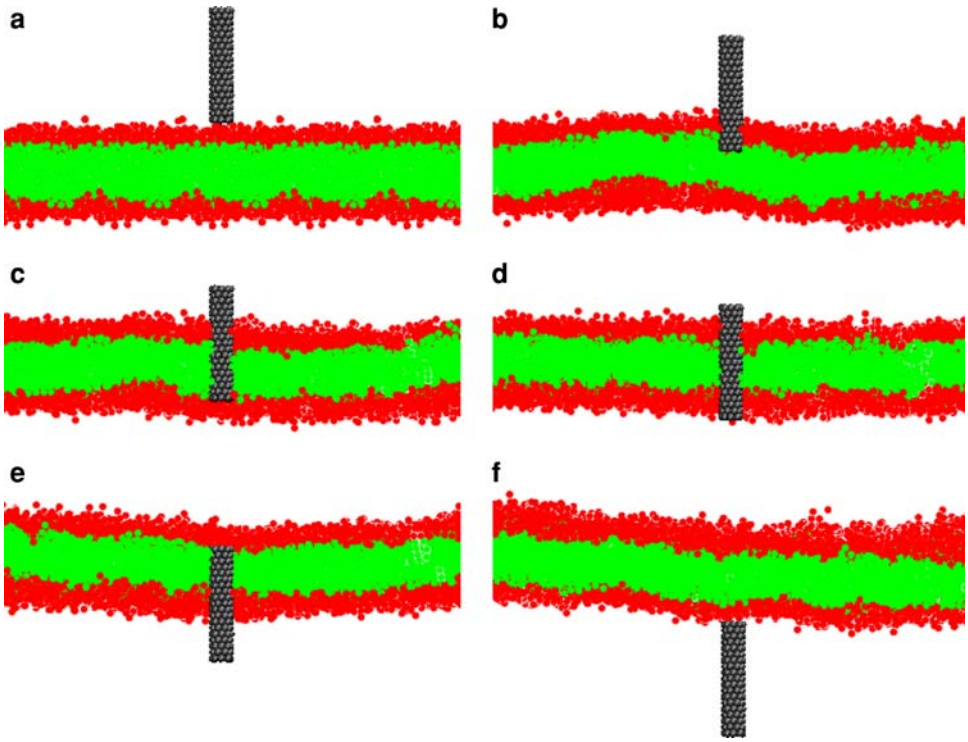

Fig. 5 Time sequence of six snapshots of a (single-walled) nanotube piercing through a membrane driven by the van der Waal force

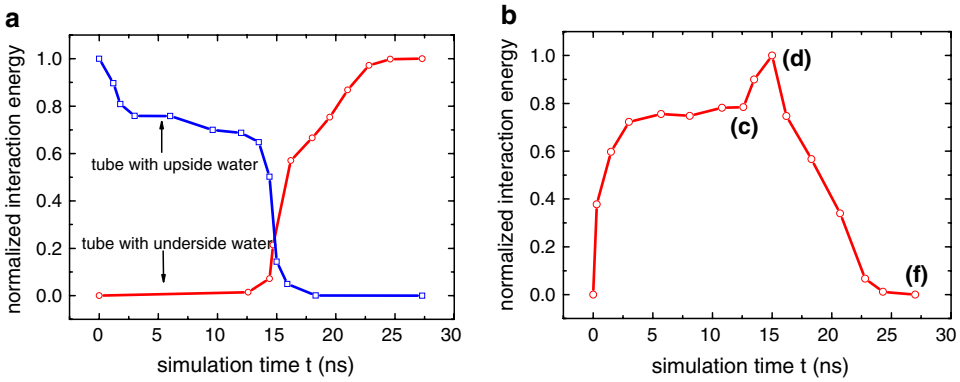

Fig. 6 **a** Interaction energy (normalized by the maximum interaction energy with corresponding interaction parameters) between the (single-walled) nanotube and water as a function of time during piercing. The *blue line* corresponds to interaction between the nanotube and water above the bilayer, while the *red line* corresponds to interaction between the nanotube and water below the bilayer. **b** Normalized interaction energy of the nanotube with lipid molecules as a function of time. The letter c, d, and f indicate the states shown in Fig. 5

models to describe the wrapping and piercing mechanisms. It is well known that the lipid bilayer behaves like a two dimensional fluid in the plane of the membrane and a bending-resistant solid in the third dimension. In the wrapping process, the bilayer undergoes large deformation with rearrangement of lipid molecules to form a cylindrical shape. In the piercing process, the lipid molecules beneath the bottom end of the tube are squeezed outwards by the piercing tube. We propose two different theoretical models to describe these two entry mechanisms.

For the wrapping mechanism, we model the lipid bilayer as a two dimensional incompressible viscous fluid with fixed thickness h in the third dimension. Consider an infinite flat bilayer wrapping around a nanotube with radius R. In cylindrical coordinates (Fig. 7), the components of the rate of deformation tensor are expressed as

$$V_r = \frac{\partial v_r}{\partial r}, \qquad V_\theta = \frac{1}{r}\frac{\partial v_\theta}{\partial \theta} + \frac{v_r}{r} = \frac{v_r}{r}, \tag{1}$$

where v_r and v_θ are the radial and circumferential velocities of the planar membrane, respectively (Fig. 7a). Because of the axisymmetry, v_θ should not change along the circumfe-

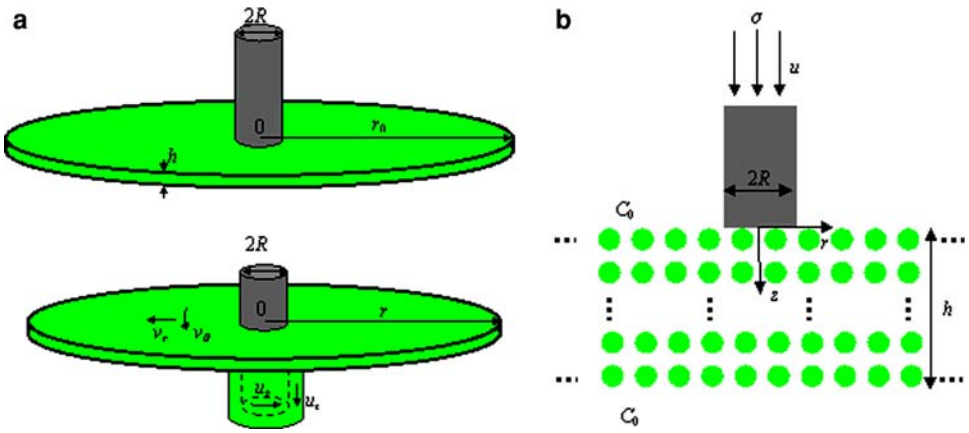

Fig. 7 The theoretical models for wrapping and piercing of nanotubes into cell. **a** Schematic illustration of cell membrane wrapping around the tube. The membrane is considered as a two dimensional viscous fluid with fixed thickness h in the third dimension. **b** Schematic illustration of a vacancy diffusion model for a cylindrical tube indenting a bilayer under stress σ

rential direction. On the other hand, in-plane incompressibility requires

$$V_r + V_\theta = \frac{\partial v_r}{\partial r} + \frac{v_r}{r} = 0, \tag{2}$$

and Eq. (1) is simplified as

$$V_r = -\frac{v_r}{r}, \qquad V_\theta = \frac{v_r}{r}, \tag{3}$$

with the radial velocity related with radius by

$$r v_r = C_1, \tag{4}$$

where C_1 is a constant.

For the part of membrane which is wrapped around the nanotube, the velocity components are denoted as u_z and u_s (Fig. 7a) which satisfy the continuity condition

$$\partial u_z/\partial z + \partial u_s/\partial s = 0. \tag{5}$$

Due to the axisymmetry, both u_s and u_z should not change along the circumference of tube. Thus this part of the membrane has no shear deformation and simply flows at a constant rate, making no contribution to the viscous dissipation. If there is no slipping between the nanotube and the membrane in the wrapping process, the entry velocity of the nanotube is then given by u_z. Given the condition that there is no surface area change during the deformation of membrane, we obtain

$$\pi r_0^2 = \pi r_e^2 + 2\pi(R + h/2)L, \tag{6}$$

where r_0 and r_e are the initial and deformed dimensions of membrane and L is the wrapping depth of the nanotube. The time rate of change of Eq. (6) gives

$$r_e \dot{r}_e = r_e v_{re} = -(R + h/2)\dot{L} = -(R + h/2)u_z. \tag{7}$$

It follows directly from Eqs. (4) and (7) that

$$r v_r = -(R + h/2)u_z. \tag{8}$$

The rate of viscous dissipation per unit volume during the deformation of membrane is given by [29]

$$\phi = 4\eta(v_r/r)^2 = 4\eta\left(\frac{(R + h/2)u_z}{r^2}\right)^2, \tag{9}$$

where η is the viscosity of the bilayer. Integrating Eq. (9) on the entire plane of the bilayer, we obtain the rate of viscous dissipation associated with the viscous deformation of the membrane as

$$\Phi = \int_V \phi \mathrm{d}V = \int_{R+h/2}^{r_e} 4\eta\left(\frac{(R + h/2)u_z}{r^2}\right)^2 h \cdot 2\pi r' \mathrm{d}r'. \tag{10}$$

On the other hand, the free energy change during the wrapping process is given by

$$F = \left(\frac{1}{2}k_c c^2 - \Delta\gamma\right) \cdot 2\pi(R + h/2)L, \tag{11}$$

where k_c is the bending modulus, $c = 1/(R + h/2)$ is the curvature of wrapped bilayer and $\Delta\gamma$ is the work of adhesion between the nanotube and the bilayer. The power balance during the wrapping of the tube requires

$$\Phi = -\mathrm{d}F/\mathrm{d}t. \tag{12}$$

Combining Eqs. (6), (10), (11) and (12) yields

$$u_z = \frac{\Delta\gamma(R + h/2)}{2\eta h}\left(1 - \frac{1}{2}\frac{k_c}{\Delta\gamma(R + h/2)^2}\right) \times \left(\frac{r_0^2 - 2(R + h/2)L}{r_0^2 - 2(R + h/2)L - (R + h/2)^2}\right). \tag{13}$$

Since the overall size of the membrane is much larger than the tube, for simplicity we assume $r_0 \to \infty$ and simplify Eq. (11) as

$$u_z \approx \frac{\Delta\gamma(R + h/2)}{2\eta h}\left(1 - \frac{1}{2}\frac{k_c}{\Delta\gamma(R + h/2)^2}\right). \tag{14}$$

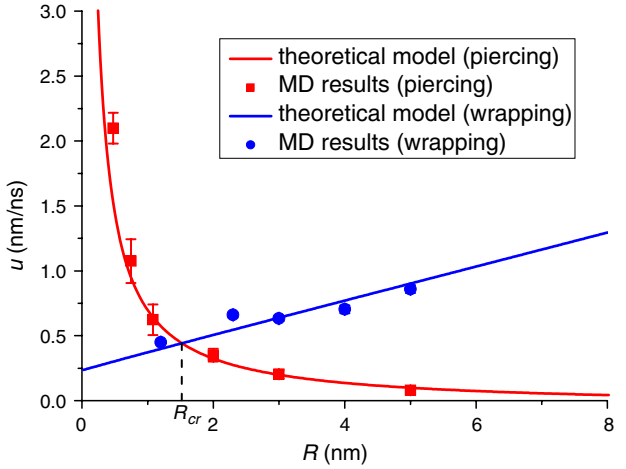

Fig. 8 The rates of entry associated with wrapping and piercing of nanotubes as a function of the tubes radius. The *blue line* denotes the theoretical model for the wrapping case and the *red* one denotes that for the piercing case. The *blue dots* denote the CGMD simulation results for the wrapping mode of entry and the *red dots* denote simulation results for the piercing mode of entry. The intersection of the two lines gives rise to a critical size for transition

To check the reliability of this model in describing the wrapping process, a series of MD simulations with nanotubes of different radii are performed and the wrapping rates are shown in Fig. 8, together with Eq. (14) where the parameters are chosen as $h = 4\,\text{nm}$, $\Delta\gamma/2\eta = 0.52\,\text{nm/ns}$ and $k_c/2\Delta\gamma = 0.35\,\text{nm}^2$. We emphasize that these are reasonable values since the bending modulus is about $4 \times 10^{-20}\,\text{J}$ [23,30], the viscosity of membrane at 323 K is about $15 \times 10^{-3}\,\text{Pa s}$ [31] and the work of adhesion in our simulations is about 0.047 N/m.

For the piercing mode of entry, we adopt a vacancy diffusion model which has been previously developed to describe impression induced creep of a thin film [32]. Figure 7b shows a cylindrical punch being pushed into the bilayer with velocity u under stress σ. The two free surfaces of the membrane are assumed to be a constant source of vacancies with concentration C_0. Considering steady state vacancy diffusion, we write Fick's second law

$$D_r \frac{1}{r}\frac{\partial}{\partial r}\left(r\frac{\partial C}{\partial r}\right) + D_z \frac{\partial^2 C}{\partial Z^2} = 0, \quad 0 < Z < h, \tag{15}$$

with associated boundary conditions

$$C = C_0, \quad Z = 0, \quad r > R, \tag{16a}$$

$$C = C_0, \quad Z = h, \tag{16b}$$

$$\frac{\partial C}{\partial Z} = \frac{u}{\Omega D_z}, \quad Z = 0, \quad 0 < r < R, \tag{16c}$$

where D_r and D_z are vacancy diffusion coefficients in the radial (r) and vertical (z) directions, and Ω is the molar volume of the diffusion species. During the piercing, the mechanical work due to punch stress is transformed into the chemical energy as

$$\frac{N_A k_B T}{\pi R^2}\int_S \ln\left(\frac{C_0}{C(r,0)}\right) \mathrm{d}s = \sigma\Omega, \tag{17}$$

where N_A is Avogadro's number, k_B is Boltzmann's constant, T is the temperature and S the area of the cross section area of the punch. Solving the above equations gives

$$u = u^* f(\chi)\chi, \tag{18}$$

where $u^* = \frac{3\pi\Omega^2 C_0 \sigma D_z}{4N_A k_B T h}$, $\chi = \alpha h/R$, $\alpha = \sqrt{D_r/D_z}$ and

$$\frac{1}{f(\chi)} = 1 - \frac{\xi(3)}{3\pi}\chi^{-3} + \frac{2\xi(5)}{5\pi}\chi^{-5} + \frac{1}{9}\left(\frac{\xi(3)}{\pi}\right)^2 \chi^{-6} + O(\chi^{-7}), \tag{19}$$

$\xi(n)$ being the Riemann zeta function. Equation (19) is an asymptotic series which converges with the condition $\chi > 1$. In present study the mobility of lipid molecules in the bilayer is usually much larger in the lateral direction (intermembrane diffusion) than in the vertical direction (flip-flop), suggesting $\alpha \gg 1$. For nanotubes with radius comparable to the thickness of the bilayer, χ is much larger than 1 and as discussed in Ref. [32], Eq. (19) would converge to 1 and the rate of piercing becomes inversely proportional to the radius of the tube. To check the validity of this model, CGMD simulations are performed with tubes of different radii piercing into the membrane (the degrees of freedom of some lipid molecules in the direction perpendicular to the plane of the bilayer is constrained to prevent them from wrapping around the tube). Figure 8 shows that the theoretical model fits the CGMD results if the parameters in Eq. (18) are chosen such that $u^*\alpha h = 0.75\,\text{nm}^2/\text{ns}$, i.e. $u = 0.75/R$.

Figure 8 shows that the observed change of pathway from wrapping to piercing as the radius of the nanotube is reduced to below a critical size may be understood from a kinetic competition between the two modes of entry. For piercing, the rate of entry is governed by the diffusivity of lipid molecules beneath the nanotube to be pushed outward by the tube. In contrast, for wrapping, the rate of entry is controlled by the viscous flow of lipid molecules near the nanotube to wrap around the tube. Below the critical radius R_{cr}, the piercing mode is faster due to small distance of diffusion underneath the tube while the wrapping mode becomes less favorable due to the high curvature associated with wrapping. Above the critical radius, the wrapping mode becomes dominant compared to piercing as the curvature energy is reduced and the diffusion distance is extended. In this way, the radius of the nanotube plays an important role in selecting the pathway of entry into a cell.

4 Conclusions

Through coarse grained molecular dynamics simulations and theoretical models, we have shown that, depending on the radius, a carbon nanotube can enter a cell either by wrapping into the cell membrane or by directly piercing through the membrane. Both van der Waals and hydrophobic forces are found to be important in these processes. A critical radius exists for the transition between the two modes of entry: sufficiently small tubes favor piercing due to small diffusion distance and large curvature energy, while larger tubes favor wrapping due to larger diffusion distance and lower curvature energy.

The limitation of this work is that we have artificially set the interaction parameters between CNT's and the lipid head group (level I and II). Since chemically pure CNT's are hydrophobic and should have weak interactions with the hydrophilic head groups of lipids, our selection of interaction parameters may have overestimated the interactions between CNT's and the bilayer. The justifications for this set-up are that CNT's entering cells are commonly functionalized and we are primarily interested in the effects of their geometry on tube-bilayer interaction. In other words, we have considered interaction parameters that are only appropriate for decorated CNT's in our CGMD simulations.

Compared to viruses entering cells via endocytosis, there are some similarities and differences for the observed entry mechanisms of carbon nanotubes. Viruses usually enter animal cells via a wrapping process mediated by specific adhesion with receptors and aided by protein coats in the membrane. As a consequence, the wrapping of viruses may be highly dependent on factors such as the temperature and the concentration and diffusivity of receptors and clathrin. In contrast, the slender geometry and perfect atomic structure of carbon nanotubes make them capable of adhering to lipid membranes via non-specific adhesion via van der Waals force. Such non-specific adhesion is less sensitive to temperature and other environmental factors. Nevertheless, the later stage of the wrapping of nanotubes may require the action of energy consuming motor molecules to facilitate the fission process, similar to endocytosis. It has been found that there exists an optimal particle size for the fastest entry in receptor-mediated endocytosis (see, e.g. [33]). In the present work, we have found another interesting size effect for carbon nanotubes: the radius of the nanotube determines the selection of entry pathway. Sufficiently thin nanotubes can pierce through the membrane while larger nanotubes tend to enter cells via wrapping mediated by non-specific adhesion. Bearing in mind that living cells are covered with glycocalyx, there should be an upper size limit above which the tube will no longer be able to effectively reach the surface of the bilayer. Therefore, we suggest there is a size window within which a nanotube will tend to enter cells via wrapping.

References

1. Moghimi, S.M., Szebeni, J.: Stealth liposomes and long circulating nanoparticles: critical issues in pharmacokinetics, opsonization and protein-binding properties. Prog. Lipid Res. **42**, 463–478 (2003)
2. Takeuchi, H., Yamamoto, H., Kawashima, Y.: Mucoadohesive nanoparticulate systems for peptide drug delivery. Adv. Drug Deliv. Rev. **47**, 39–54 (2001)
3. Muller, R.H., Jacobs, C., Kayser, O.: Nanosuspensions as particulate drug formulations in therapy. Rationale for development and what we can expect for the future. Adv. Drug Deliv. Rev. **47**, 3–19 (2001)
4. Kumar, M.N.V.R., Hellermann, G., Lockey, R.F., Mohapatra, S.S.: Nanoparticle-mediated gene delivery: state of the art. Expert Opin. Biol. Ther. **4**, 1213–1224 (2004)
5. Alivisatos, P.: The use of nanocrystals in biological detection. Nat. Biotechnol. **22**, 47–52 (2004)
6. Penn, S.G., He, L., Natan, M.J.: Nanoparticles for bioanalysis. Curr. Opin. Chem. Biol. **7**, 609–615 (2003)
7. Drummond, T.G., Hill, M.G., Barton, J.K.: Electrochemical DNA sensors. Nat. Biotechnol. **21**, 1192–1199 (2003)
8. Cui, D.X., Tian, F.R., Ozkan, C., Wang, M., Gao, H.J.: Titel effect of single wall carbon nanotubes on human HEK293 cells. Toxicol. Lett. **155**, 73–85 (2005)
9. Monteiro-Riviere, N.A., Nemanich, R.J., Inman, A.O., Wang, Y.Y., Riviere, J.E.: Multi-walled carbon nanotube interactions with human epidermal keratinocytes. Toxicol. Lett. **155**, 377–384 (2005)
10. Kam, N.W.S., Jessop, T.C., Wender, P.A., Dai, H.J.: Nanotube molecular transporters: internalization of carbon nanotube-protein conjugates into mammalian cells. J. Am. Chem. Soc. **126**, 6850–6851 (2004)
11. Kam, N.W.S., Dai, H.J.: Carbon nanotubes as intracellular protein transporters: generality and biological functionality. J. Am. Chem. Soc. **127**, 6021–6026 (2005)
12. Kam, N.W.S., O'Connell, M., Wisdom, J.A., Dai, H.J.: Carbon nanotubes as multifunctional biological transporters and near-infrared agents for selective cancer cell destruction. Proc. Natl. Acad. Sci. USA **102**, 11600–11605 (2005)
13. Cherukuri, P., Bachilo, S.M., Litovsky, S.H., Weisman, R.B.: Near-infrared fluorescence microscopy of single-walled carbon nanotubes in phagocytic cells. J. Am. Chem. Soc. **126**, 15638–15639 (2004)
14. Pantarotto, D., Briand, J., Prato, M., Bianco, A.: Translocation of bioactive peptides across cell membranes by carbon nanotubes. Chem. Commun. **1**, 16–17 (2004)
15. Lu, Q., Moore, J.M., Huang, G., et al.: RNA polymer translocation with single-walled carbon nanotubes. Nano Lett. **4**, 2473–2477 (2004)
16. Bianco, A., Hoebeke, J., godefroy, S., et al.: Cationic carbon nanotubes bind to CpG oligodeoxynucleotides and enhance their immunostimulatory properties. J. Am. Chem. Soc. **127**, 58–59 (2005)
17. Smit, B., Esselink, K., Hibers, P.A.J., et al.: Computer simulations of surfactant self-assembly. Langmuir **9**, 9–11 (1993)
18. Palmer, B.J., Liu, J.: Simulations of micelle self-assembly in surfactant solutions. Langmuir **12**, 746–753 (1996)
19. Goetz, R., Lipowsky, R.: Computer simulations of bilayer membranes: self-assembly and interfacial tension. J. Chem. Phys. **108**, 7397–7409 (1998)
20. Den Otter, W.K., Briels, W.J.: The bending rigidity of an amphiphilic bilayer from equilibrium and nonequilibrium molecular dynamics. J. Chem. Phys. **118**, 4712–4720 (2003)
21. Von Gottberg, F.K., Smith, K.A., Hatton, T.A.: Stochastic dynamics simulation of surfactant self-assembly. J. Chem. Phys. **106**, 9850–9857 (1997)

22. Noguchi, H., Takasu, M.: Self-assembly of amphiphiles into vesicles: a Brownian dynamics simulation. Phys. Rev. E **64**, 041913–041919 (2001)
23. Marrink, S.J., de Vries, A.H., Mark, A.E.: Coarse grained model for semiquantitative lipid simulations. J. Phys. Chem. B **108**, 750–760 (2004)
24. Berendsen, H.J.C., Postma, J.P.M., DiNola, A., Haak, J.R.: Molecular dynamics with coupling to an external bath. J. Comp. Phys. **81**, 3684–3690 (1984)
25. Berendsen, H.J.C., van der Spoel, D., van Drunen, R.: GROMACS: a message-passing parallel molecular dynamics implementation. Comput. Phys. Commun. **91**, 43–56 (1995)
26. Jahn, R., Lang, T., Sudhof, T.C.: Membrane fusion. Cell **112**, 519–533 (2003)
27. White, J.M.: Viral and cellular membrane-fusion proteins. Annu. Rev. Physiol. **52**, 675–697 (1990)
28. Lopez, C.F., Nielsen, S.O., Moore, P.B., Klein, M.L.: Understanding nature's design for a nanosyringe. Proc. Natl. Acad. Sci. USA **101**, 4431–4434 (2004)
29. Evans, E.A., Skalak, R.: Mechanics and thermodynamics of biomembranes. CRC Crit. Rev. Bioeng. **3**, 181–330 (1979)
30. Rawicz, W., Olbrich, K.C., Mcintosh, T., et al.: Effect of chain length and unsaturation on elasticity of lipid bilayers. Biophys. J. **79**, 328–339 (2000)
31. Turley, W.D., Offen, H.W.: Lipid microviscosity of DMPC vesicles at high pressure. Dipyrenylpropane excimer fluorescence. J. Phys. Chem. **90**, 1967–1970 (1986)
32. Yang, F.Q., Li, J.C.M.: Impression creep of a thin film by vacancy diffusion. II. Cylindrical punch. J. Appl. Phys. **74**, 4390–4397 (1993)
33. Gao, H., Shi, W., Freund, L.B.: Mechanics of receptor-mediated endocytosis. Proc. Natl. Acad. Sci. USA **102**, 9469–9474 (2005)